ATMOSPHERIC SCIENCE

North American April tornado occurrences linked to global sea surface temperature anomalies

J.-E. Chu[1,2], A. Timmermann[1,2]*, J.-Y. Lee[1,3]

Annual tornado occurrences over North America display large interannual variability and a statistical linkage to sea surface temperature (SST) anomalies. However, the underlying physical mechanisms for this connection and its modulation in a rapidly varying seasonal environment still remain elusive. Using tornado data over the United States from 1954 to 2016 in combination with SST-forced atmospheric general circulation models, we show a robust dynamical linkage between global SST conditions in April, the emergence of the Pacific-North American teleconnection pattern (PNA), and the year-to-year tornado activity in the Southern Great Plains (SGP) region of the United States. Contrasting previous studies, we find that only in April SST-driven atmospheric circulation anomalies can effectively control the northward moisture-laden flow from the Gulf of Mexico, boosting low-level moisture flux convergence over the SGP. These strong large-scale connections are absent in other months because of the strong seasonality of the PNA and background moisture conditions.

INTRODUCTION

2011 was an extremely active tornado year over North America (*1*), with nearly 1700 recorded tornadoes, resulting in more than 500 fatalities and $10 billion property and crop losses (www.spc.noaa. gov/wcm/2011-NOAA-NWS-tornado-facts.pdf). Yet, the subsequent tornado season in 2012 was relatively quiet, with an estimated 900 tornadoes and 70 fatalities (www.spc.noaa.gov/wcm/2012/2012-NOAA-NWS-tornado-facts.pdf). In both years, most tornadoes occurred in April, 1 month before the climatological peak conditions. This observation raises the important question as to whether the year-to-year variations in tornado occurrences over North America, and particularly over the very active Southern Great Plains (SGP) region, can be partly explained by potentially predictable low-frequency climatic processes (fig. S1), such as large-scale sea surface temperature anomalies (SSTA), and whether there are month-to-month differences in the effect of large-scale conditions on submesoscale weather variability.

Peaking in April and May (fig. S2), supercell thunderstorms and tornado activity increase along the southeastern side of the Rocky Mountains, when moisture-laden air is transported from the relatively warm Gulf of Mexico by the low-level meridional jet (*2*). The current generation of global atmosphere models lacks the ability to simulate individual tornadoes. It is therefore necessary to use statistical methods to determine which large-scale and synoptic-scale atmospheric conditions are favorable for tornado generation. Key insights into tornadic environments have been provided by sounding data (*3*) and radar observations, which show that most of SGP tornadoes are spawned by mesoscale convective systems, commonly referred to as right-moving supercell thunderstorms (*4*).

Previous studies have identified statistical linkages between tornado occurrences and supercell thunderstorm activity in the Great Plains region to atmospheric pressure anomalies near the Rocky Mountains (*5*, *6*), dry lines (*7*), the North American low-level jet (*8*, *9*), the Madden-Julian Oscillation (*10–12*), the El Niño–Southern

Oscillation (ENSO) (*5*, *13–16*), and SSTA over the Gulf of Mexico (*17*, *18*). More specifically, changes in April and May tornado numbers over the United States during the past 60 years appear to be linked to anomalous zonal gradients of equatorial Pacific SSTA (*13*). Other studies highlighted a relationship between four dominant springtime ENSO phases and U.S. tornado outbreaks in February to May (*14*). These findings demonstrate that ENSO may serve as a powerful modulator of tornado statistics, potentially providing a source of seasonal predictability. Although the underlying statistical evidence is encouraging, a clear physical picture that links SSTA, stationary waves, and tornado activity has not yet fully emerged. Because the influence of the ENSO phenomenon on North America through the Pacific-North American (PNA) teleconnection pattern (*19–21*) is strongly suppressed during boreal summer (fig. S3), a better physical understanding requires careful consideration of seasonal and even month-to-month atmospheric variations. This is further underscored by the finding that, under the rapidly changing spring background states over the Great Plains region, atmospheric instability as quantified by the convective available potential energy (CAPE) is nearly doubled in May compared to April.

Here, we further elucidate the physical mechanism responsible for the subseasonally modulated relationship between tropical and extratropical SSTA, large-scale stationary wave anomalies, and tornado frequencies in boreal spring (fig. S1). Using 22 SSTA-forced atmospheric general circulation model (AGCM) simulations forced by the observed sea surface temperatures (SST) (*22*) (table S1), we first evaluate the impacts of large-scale SSTA patterns on the generation of stationary waves in April and May. We then explore how these large-scale factors influence synoptic systems and mesoscale events. Our analysis is based on a recent compilation of tornado counts over North America from 1954 to 2016 taken from the Storm Prediction Center (SPC) (www.spc.noaa.gov/gis/svrgis/) and a monthly mean temporal and spatial interpolation of total numbers of EF1 to EF5 tornadoes onto a 1° × 1° grid covering North America. To include a representative portion of high climatological tornado occurrences, we define the SGP region here as 30°N to 40°N and 100°W to 90°W. Climatological numbers of tornadoes in the SGP peak in April and May. Furthermore, interannual variations of tornado numbers in April and May in the SGP are essentially uncorrelated (fig. S2). Given these conditions,

[1]Center for Climate Physics, Institute for Basic Science (IBS), Busan 46241, South Korea. [2]Pusan National University, Busan 46241, South Korea. [3]Department of Climate System and Research Center for Climate Sciences, Pusan National University, Busan 46241, South Korea.
*Corresponding author. Email: timmermann@pusan.ac.kr

we conduct a monthly stratified analysis of tornado data, focusing on April and May separately.

RESULTS

SST-forced atmospheric variability in April and May

Wintertime midlatitude atmospheric variability over the North Pacific and North America is strongly controlled by the low-frequency PNA pattern. The PNA is an intrinsic mode of atmospheric variability that arises from the interaction between the climatological mean flow and high-frequency eddy activity and that can get further excited by the presence of ENSO-related diabatic atmospheric forcing (19–21).

To estimate the SST-driven atmospheric variability in April and May, we used the multimodel ensemble of 22 SST-forced atmospheric model simulations from the Atmospheric Model Intercomparison Project (AMIP) (23, 24). AMIP simulations were conducted under the auspices of the CMIP5 (Coupled Model Intercomparison Project, phase 5) (22). The AMIP runs are based on AGCM simulations forced by observed SST and sea ice conditions, and they cover the period from 1980 to 2008. For the analysis of the AMIP simulations, monthly SSTs and geopotential height fields at 500 hPa were interpolated for each model to a common spatial resolution of 2.5° × 2.5° latitude by longitude. Before the analysis, long-term linear trends were removed from all datasets. To investigate the dominant pattern of SST-driven atmospheric variability (stationary waves in fig. S1), we used maximum covariance analysis based on a singular value decomposition (SVD) of observed 500-hPa geopotential height anomalies (Z_{500}'), estimated from the National Centers for Environmental Prediction (NCEP)/National Center for Atmospheric Research (NCAR) reanalysis version 1 (NCEP1) (25), and AMIP-simulated Z_{500}' values over 20°N to 70°N and 0°E to 360°E in April and May (see Materials and Methods). By construction, the leading mode of covariance between observations and SST-forced model simulations is only due to the SSTA-forced part of atmospheric variability. Non-SST–related variability cannot be covariant between the AMIP simulations and the reanalysis data. Remaining noise sources in our analysis are further eliminated by calculating the 22-member ensemble mean of simulated AMIP fields before the SVD analysis.

Figure 1 (A to D) shows the linear regression coefficients of the large-scale SSTA conditions from the Extended Reconstructed Sea Surface Temperature version 5 (ERSSTv5) (26) and Z_{500}' from NCEP1 onto the corresponding expansion coefficients of the leading SVD mode.

In April, a teleconnection pattern—characterized by mid-tropospheric geopotential height anomalies, which extend from the central North Pacific to eastern North America—explains the largest amount of SSTA-induced anomalous atmospheric variability (Fig. 1, A and C). Consistent with the negative phase of the PNA, this pattern features below-average pressure in the vicinity of the Hawaiian Islands and over the West Coast of the United States, as well as above-average pressure south of the Aleutian Islands and over the southeastern United States. The negative phase of the PNA can be excited by changes in tropical convection due to La Niña (27) and/or barotropic wave amplification of high-frequency eddy forcing (28). In our analysis, the associated SSTA pattern is characterized by negative temperature anomalies in the central Pacific and along the west coast of North America and positive temperature anomalies in the subtropical Pacific and the Gulf of Mexico. In May, the central
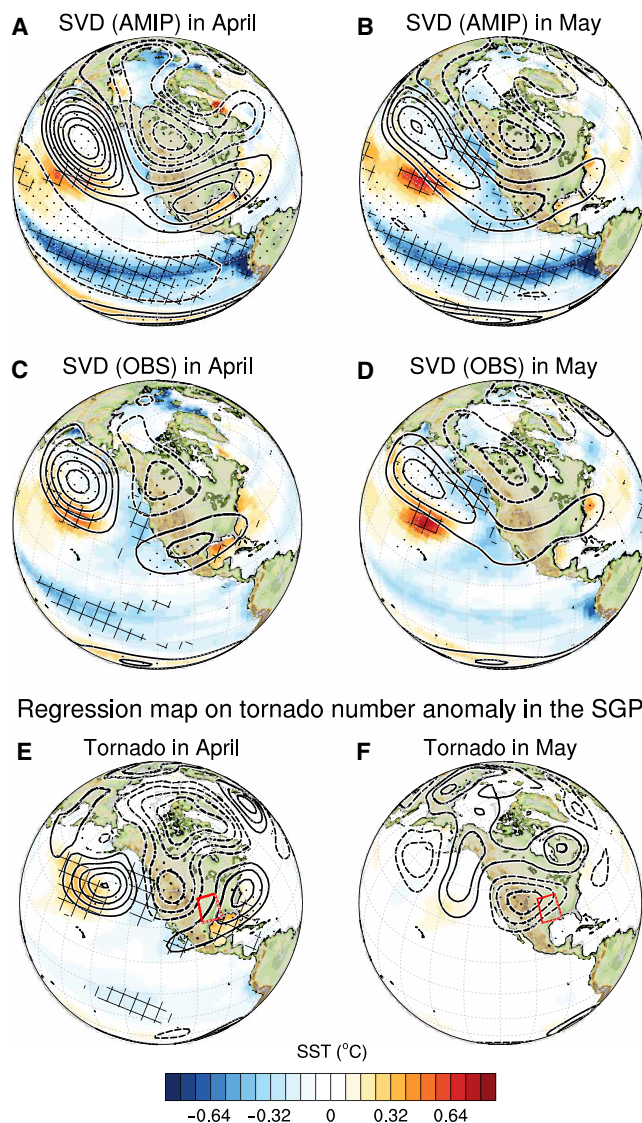
Homogeneous regression map for SVD1: Z_{500}' (AMIP, OBS)

Regression map on tornado number anomaly in the SGP

Fig. 1. Influence of SSTA on the atmosphere and its relationship with US. tornado activity in April and May. (**A** to **D**) The SVD analysis is conducted on the basis of AMIP-simulated and NCEP1 reanalysis (OBS) year-to-year variabilities of the 500-hPa geopotential height anomalies (Z_{500}') over the northern hemisphere (20°N to 70°N and 0°E to 360°E) for April (A and C) and May (B and D), respectively (see Materials and Methods). (**E** and **F**) Regressed patterns of Z_{500}' and SSTAs on tornado numbers aggregated over the SGP region (30°N to 40°N and 100°W to 90°W; red box) for April (left) and May (right). Solid (dashed) lines indicate positive (negative) values. The intervals are 0.08 K for SSTA and 4 m for Z_{500}'. The stippled (cross-hatched) areas indicate values for which the local null hypothesis of zero regression can be rejected at the 95% level for Z_{500}' (SSTA), based on a Student's t test with 27 and 61 degrees of freedom for AMIP and observations, respectively. Long-term linear trends were removed before statistical analysis.

Pacific Z_{500}' anomaly pattern is squeezed meridionally as the center of the Pacific jet stream moves from the west to the central Pacific, generating zonally elongated positive height anomalies from the North Pacific to eastern North America and negative anomalies
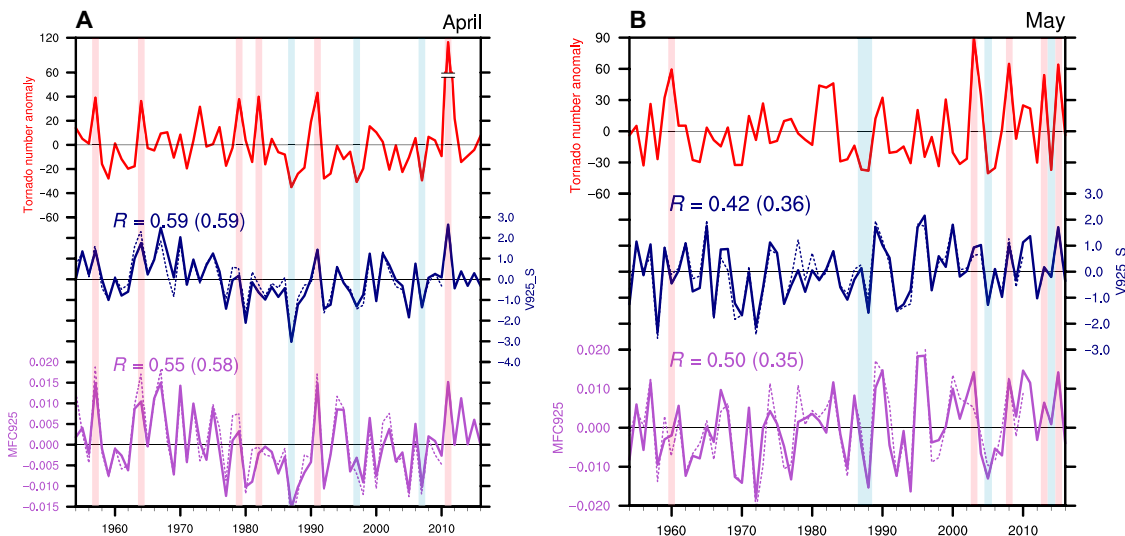
Fig. 2. Year-to-year changes in the number of tornadoes, low-level jet, and moisture flux convergence over the SGP. Observed tornado number anomalies over the SGP region (red), meridional wind anomalies (blue) over the south of the SGP (V925_S, in meters per second; 20°N to 30°N and 100°W to 90°W), and moisture flux convergence anomalies at 925 hPa (MFC925, 10^{-3} g/kg per second) over the SGP (purple) from 1954 to 2016 for (**A**) April and (**B**) May. The V925_S and MFC925 were calculated on the basis of two datasets—NCEP1 (solid line) and European Centre for Medium-Range Weather Forecasts 20th century reanalysis (ERA-20C; dashed line). Correlation coefficients (*R*) between tornado number anomalies and climate indices are shown in the top left corner (*R* values with ERA-20C are in braces). Long-term linear trends were removed.

centered in western Canada (Fig. 1, B and D). The monthly variances in the leading mode of SST-driven atmospheric Z_{500}' variability in April and May amount to 41 and 54% of the total variance, respectively.

Dynamic link between tornado activity and SST-forced pattern

The SVD results (Fig. 1, A to D) imply that there are distinct atmospheric patterns in the 500-hPa geopotential height field induced by SSTA in April and May. In particular, previous studies found that the presence of the 500-hPa trough over the northwestern United States and associated southwesterly flow oftentimes correspond to high tornado occurrences (*5*, *6*). While these studies have noted the relationship between upper-level atmospheric wave patterns and interannual variability of tornado activity during the peak tornado season, no systematic study has been carried out to assess month-to-month differences in this dynamic linkage. To better understand the relationship between tornado number anomalies in the SGP in April and May and both large-scale SSTA and Z_{500}' conditions, we calculated the associated monthly regression coefficients.

For May, we found no statistically significant connection between tornado numbers and large-scale atmospheric flow and SST patterns (Fig. 1F). By contrast, in April, we found statistically significant connections between tornado numbers and both SSTA and Z_{500}' (Fig. 1E). The regression pattern analysis shows that more frequent SGP tornado occurrences in April are typically associated with equatorial Pacific and eastern North Pacific cooling (*14*), as well as positive temperature anomalies in the subtropical Pacific and tropical western Atlantic. High tornado activity in April is also related to an atmospheric stationary wave pattern over North America (Fig. 1E), which is consistent with a negative PNA-like pattern (Fig. 1, A and C), identified through the SVD analysis as the dominant mode of SST-forced variability. To demonstrate the statistical significance of the regression maps of SSTAs and Z_{500}' on tornado number anomalies in April, we conducted a statistical field significance test using 1000 regression

maps obtained by using randomly generated time series and found that both SSTA and Z_{500}' regression maps in April (Fig. 1E) exceed the probability of random sampling, whereas those for May are not statistically significant (for more details on the field significance test, see Materials and Methods and fig. S4).

We further examine the statistical connections between tornado frequencies over SGP and regional averages of two atmospheric variables—low-level meridional wind anomalies at 925 hPa averaged over the south of the SGP (V925_S) and moisture flux convergence anomalies at 925 hPa (MFC925) averaged over the SGP (Fig. 2). The correlation coefficient values between tornado frequencies and these time series in April attain values of 0.55 to 0.59. This result implies that ~30 to 35% of the variance in the number of tornadoes in April is caused by large-scale atmospheric circulation patterns. The corresponding analysis for May shows a weaker connection with correlation values of 0.35 to 0.50 and considerable differences among the datasets (Fig. 2B). The statistically significant relationship between tornado number anomalies in the SGP and the atmospheric teleconnection pattern can be understood in physical terms through the increased pressure gradient over the SGP region due to the cyclonic PNA flow anomaly in the northwestern United States and the anticyclonic anomaly in the southeastern United States (Fig. 1E). The increased pressure gradient enhances the low-level jet over the southern part of the SGP, intensifying moisture convergence to the north. In addition, warm SSTA over the Gulf of Mexico funnels moist air in April into the SGP region. Moreover, vertical shear promotes the generation of tornadoes through vertical tilting of horizontal vorticity (*29*).

To further investigate the interannual drivers of the low-level jet and moisture convergence, we regressed the observed V925_S and MFC925 indices obtained in Fig. 2 onto the observed SSTA and Z_{500}' data (Fig. 3). A large-scale pattern that modulates low-level jet and moisture flux convergence in April and that closely resembles the diagnosed pattern of the conditions that are favorable for tornado generation, as described above (Fig. 1E), can be seen. It becomes
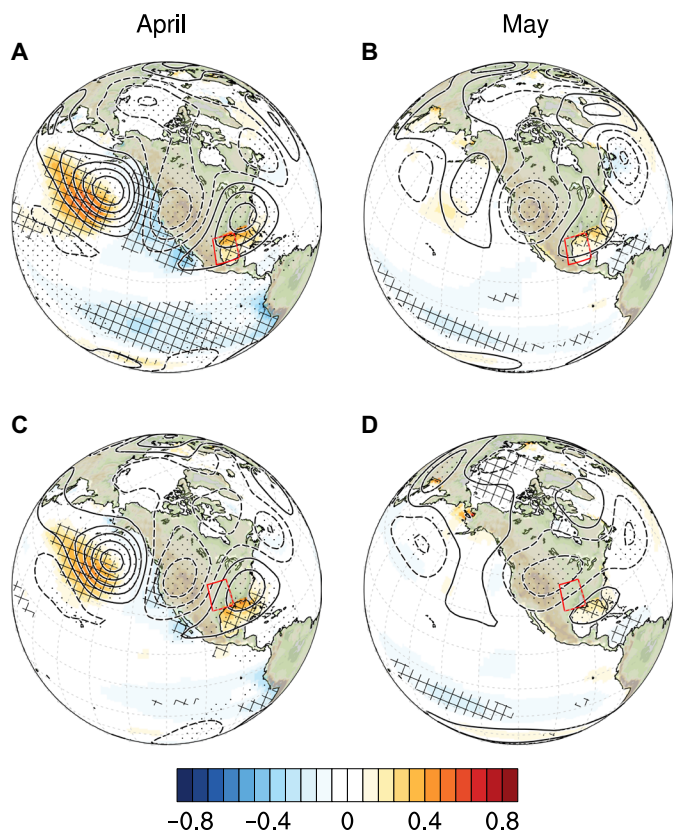
April

May

Fig. 3. Large-scale patterns controlling the low-level jet from the Gulf of Mexico and moisture over the SGP. Linear regression patterns of Z_{500}' (contour) and SSTAs (shaded areas) onto (**A** and **B**) V925_S and (**C** and **D**) MFC925 for April (left) and May (right). The contour intervals are 0.08 K for SSTA and 8 m for Z_{500}'. The stippled (cross-hatched) area indicates values for which the local null hypothesis of zero regression can be rejected at the 95% level for Z_{500}' (SSTA), based on a Student's *t* test with 61 degrees of freedom. Long-term linear trends were removed before any statistical analysis.

Fig. 4. Thermodynamic variables during strong and weak April tornado years. Monthly climatology of the (**A**) MFC925 and (**B**) cPrcp over the SGP from all years (black line), strong April tornado years (red line), and weak April tornado years (blue line). The strong (weak) April tornado years are selected on the basis of 1.5 (−1.1) SDs. The selected strong years are 1957, 1964, 1979, 1982, 1991, and 2011, and the weak years are 1959, 1987, 1992, 1997, and 2007. MFC925 is obtained from NCEP1 for 1954–2016, and cPrcp is obtained from the NARR dataset for 1979–2016. Gray-shaded area encompasses 1 SD of all years. Because of the different time frames that each dataset covers, missing years are omitted from the composite mean calculation. Two representative strong and weak tornado years are indicated by the red and blue stars, respectively.

clear that the large-scale climate patterns that are partly responsible for the interannual variations in tornado numbers in April are related to the low-level jet and moisture flux convergence over the SGP. However, such a connection is considerably weaker in May.

The connection between large-scale atmospheric flow and tornado activity in April is further supported by the strong correlation between tornado number anomalies, V925_S and MFC925, and three mesoscale environmental variables that are known to create favorable conditions for tornado generation, including CAPE, convective precipitation (cPrcp), and storm relative helicity (HLCY), which were obtained from the North American Regional Reanalysis (NARR) dataset (*30*) covering the period from 1979 to 2016 (fig. S5). Previous studies demonstrated that these variables are related to the annual cycle and spatial distribution of tornado occurrences over North America (*31*, *32*). In particular, severe supercell thunderstorms are associated with CAPE values exceeding 100 J kg^{-1} (*3*), and cPrcp and HLCY can further create conditions that are favorable for tornado generation. We found that all three variables exhibit statistically significant (>95%) correlations with variations in monthly tornado frequencies, V925_S and MFC925 in April, and the same is true for HLCY in May and June but not for cPrcp and CAPE. A statistically significant correlation value in all 3 months is found only between V925_S
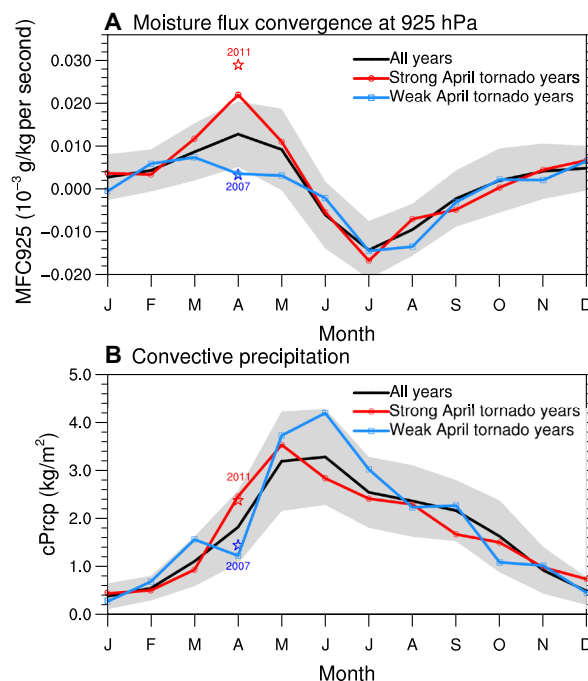
and CAPE. However, a statistically significant correlation between tornado frequencies and CAPE exists only for April. These results are due to the fact that the maximum year-to-year variance in CAPE is centered over the Gulf of Mexico, and therefore, the variability in CAPE especially in the SGP region is related to the large-scale environment that links the SGP region and the Gulf of Mexico. On the other hand, cPrcp and HLCY are associated with mesoscale supercell thunderstorms and storm tracks with maximum variance centered over the SGP. Moreover, the convective instability in the SGP region in May and June is sufficiently large to form supercell thunderstorms with values greater than 200 J kg^{-1} (fig. S6). Thus, under the condition of necessary CAPE values in May and June, kinematic factors that are commonly known to affect the occurrence of tornadoes, such as the tilting of a rotational vortex around a horizontal axis as represented by HLCY, may play a more important role in May than large-scale factors. This confirms our initial hypothesis that the month-to-month relationship between tornado frequencies and climate forcings can be different under rapidly changing spring background states.

The variance of the PNA pattern in March even exceeds that in April (fig, S3B), raising the question whether SST anomalies may also influence the statistics of tornadoes in March. However, in March, the corresponding mean climatological low-level jet is still relatively weak (fig. S7), which inhibits the production of
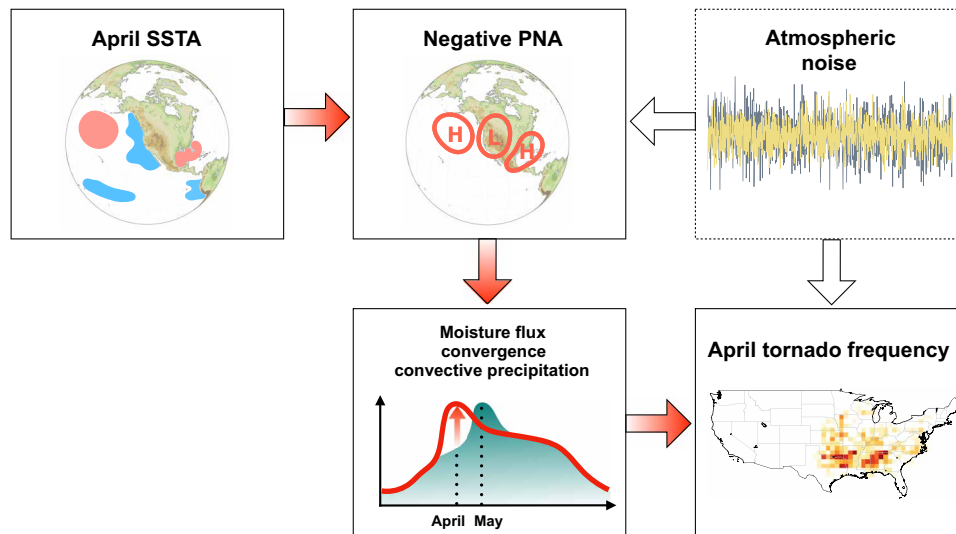
Fig. 5. Schematics illustrating enhancement in April tornado activity due to SST. Red arrows represent the sequence of the deterministic (and potentially predictable) climate influences on April tornado occurrence in the SGP region, whereas black arrows indicate unpredictable atmospheric noise. Green shading on the bottom left figure indicates the climatological annual cycle, and thick red line indicates enhancement of April mean MFC925 and cPrcp due to SST-forced atmospheric negative PNA pattern.

large-scale differential advection—one of the factors crucial for the generation of low-level wind shear over the SGP region. As a result, we expect only a weak linkage between large-scale climatic conditions and the establishment of tornadic conditions in March (fig. S7).

The role of thermodynamic and kinematic processes
The processes by which large-scale climatic conditions boost tornado occurrences in April can be understood through the enhancement of the climatological annual cycle of thermodynamic variables including MFC925 and cPrcp in the SGP region (Fig. 4). The annual cycles of MFC925 and cPrcp peak in May and June, respectively. In both variables, composites of the strong and weak April tornado years, defined here as the years with April tornado counts greater than 1.5 SDs and less than −1.1 SDs, show large amplification in their magnitude, with values exceeding the climatological mean in MFC925 and cPrcp by more than 72 and 35%, respectively. Neither May nor June data show similar enhancements in amplitude. Therefore, large-scale conditions act as a booster of low-level moisture flux convergence and cPrcp in April.

In addition to these thermodynamic constraints, kinematic conditions such as HLCY and vertical wind shear are crucial factors for tornado genesis (*31*, *32*). Our analysis demonstrates that the negative PNA stationary wave pattern significantly increases storm relative HLCY over the SGP region in April but not in May (fig. S8). This provides further evidence for a large-scale control of tornado occurrences in April through the combination of both thermodynamic and kinematic processes. The kinematic processes alone are more closely related to tornado frequencies and synoptic environments in May and June as we previously discussed in fig. S5.

Despite the strong statistical link between tornado occurrences and multiscale atmospheric process (fig. S1), most of our discussion has been based on monthly averaged statistics. To better understand the connection between tornado frequencies and shorter-scale

atmospheric phenomena, we calculated the 91-day running variance of the 6-day high-pass–filtered vertical moisture flux at 925 hPa (fig. S9). In this diagnostic, mesoscale vertical moisture flux, which is a measure of mesoscale thunderstorm activity, is intensified over the SGP region in April in very active tornado years. Again, the connection in May is strongly suppressed. If the April tornado activity were driven only by internal atmospheric noise, then we would expect there to be no significant relationship between the observed numbers of tornadoes and the intensification of weather activity, which is the case for May.

The effect of SSTA forcing on tornado activity in April is summarized schematically in Fig. 5 and fig. S1. The SSTA pattern, particularly the combination of equatorial central Pacific and eastern North Pacific cooling and central North Pacific and Gulf of Mexico warming, contributes to the formation of a negative PNA. This PNA acts as a precursor for supercell thunderstorm formation and elevated tornado genesis by preconditioning moisture supply, HLCY, and cPrcp in April. In May, however, these strong large-scale connections are absent because of the seasonality of the PNA, which weakens by a factor of 2 compared to April (fig. S3).

DISCUSSION
In contrast to previous studies that identify an influence of SST anomalies on seasonally averaged U.S. tornado frequencies, our study provides new physical insights into the subseasonal modulation of tornado occurrences due to large-scale climatic conditions and synoptic-scale interactions. The results of our analysis may help to improve prediction models for extreme weather statistics over the SGP regions. Owing to the long-term persistence of SSTA, we expect a substantially increased predictability of tornado numbers in April compared to May. Our analysis suggests that changes in tornado frequencies in May are mainly due to internal atmospheric processes, rather than due to slowly varying SST boundary conditions. However, a more comprehensive analysis is needed to further

elucidate the drivers of this variability and potential linkages, for instance, to soil moisture variations.

Previous studies have demonstrated that more predictable tornadoes in early spring (March and April) are often associated with synoptic-scale systems, whereas less predictable late spring (May) outbreaks can be traced back to mesoscale systems (33). Eighty percent of the EF1 to EF5 tornadoes occur as part of right-moving supercells with a pronounced center in the SGP region in spring with a peak in May (4). Only 20% of tornadoes derive from quasi-linear convective systems that peak in April. This suggests that subseasonal variations in tornado occurrences are driven not only by the seasonality of large-scale processes but also by the seasonality and the type of the major convective systems over the SGP region. Here, we suggest that the more predictable large-scale patterns in April may also contribute to the development of spatially more organized synoptic systems, which, in turn, may enhance the predictability of tornado outbreaks or even individual events.

Our study also provides a new context for an ongoing discussion about the linkage between increasing tornado numbers, climate variability, and climate change (34). In response to increasing greenhouse gas concentrations, tropical Pacific temperatures are expected to increase faster than subtropical temperatures (35). This enhanced equatorial warming pattern, which contrasts the more favorable La Niña conditions, may possibly reduce the occurrence of tornadoes in April. However, an overall projected increase of atmospheric moisture in the Gulf of Mexico may create more favorable conditions for supercell and tornado formation in May. How these competing factors will play out against each other is unknown. Our results imply that detection studies linking long-term anthropogenic climate change and changes in tornado numbers in the SGP region should not rely on seasonally averaged statistics but need to consider subseasonal effects.

MATERIALS AND METHODS

Tornado data
North American tornado numbers were obtained from the SPC. The time period used in our study was 1954–2016. EF is the "Enhanced Fujita (EF) scale" which replaced the "Fujita (F) scale" in 2007 and ranges from EF0 (105 to 137 km/hour wind speed) to EF5 (>322 km/hour wind speed). Because extension of the tornado detection network has introduced artificial trends in long-term tornado datasets, particularly for EF0 tornadoes (36), our analysis only focused on the EF1 to EF5 categories, which are less affected by data inhomogeneities. We calculated monthly mean total number of EF1 to EF5 tornadoes per $1° \times 1°$ grid box. Before the analysis, long-term linear trends were removed from all datasets.

The study area is defined here as 30°N to 40°N and 100°W to 90°W and is referred to as the SGP region. The area was chosen to include a representative portion of the Great Plains and "Tornado Alley" regions of the United States, which have a high climatological occurrence of tornadoes. Our region of interest accounts only for a small fraction of North America. However, this small region accounts for 44 and 45% of the U.S. total April and May EF1 to EF5 tornadoes, respectively. Moreover, correlation coefficients between SGP tornado numbers and U.S. total tornado numbers attain values of 0.79 and 0.84 in April and May, respectively. Therefore, variations in the SGP tornado activity can explain a considerable fraction of the total North American tornado variability.

Observational data
The study used monthly mean SST from ERSSTv5 for the period 1954–2016. Atmospheric variables including geopotential height, zonal and meridional winds, and specific humidity were obtained from the NCEP1 for the period 1954–2016 and from the European Centre for Medium-Range Weather Forecasts 20th century reanalysis (ERA-20C) (37) for the period 1954–2010. CAPE, cPrcp, and HLCY (0 to 3 km above ground level) were obtained from the NARR dataset (30) for the period 1979–2016.

Linear regression coefficients
To understand the dynamical relationship between tornado number anomalies [$N'(t)$] in the SGP and large-scale SSTA [$T'(x,y,t)$] and $Z_{500}'(x,y,t)$, the corresponding linear regression coefficients, $P_T(x,y) = <T'(x,y,t)N'(t)>/<N'(t)^2>$ and $P_{500}(x,y) = <Z_{500}'(x,y,t)N'(t)>/<N'(t)^2>$, were calculated. Here, <…> represents the long-term time mean at each grid point location (x and y). The regression patterns shown in Fig. 1 are $T'(x,y,t)$ and $Z_{500}'(x,y,t)$ regressed onto the standardized value of $N'(t)$. The values in Fig. 1 therefore represent characteristic changes in SSTA and Z_{500}' associated with a change in tornado numbers of 1 SD.

SVD analysis
We performed the covariance matrix between the observed Z_{500}' from NCEP1 and AMIP-simulated Z_{500}' values over the northern hemisphere (20°N to 70°N and 0°E to 360°E) for the period 1980–2008 by applying SVD analysis (38), which has been used in meteorological studies. The SVD identifies pairs of Z_{500}' pattern that maximize expansion coefficients, and therefore, the leading mode of covariance provides a measure of how strongly the observed atmospheric variability is related to the SST-forced variability. We applied SVD analysis for year-to-year Z_{500}' values for April and May, respectively. The first pairs had high correlations (0.64 for April and 0.74 for May). Then, we calculated the linear regression coefficients of the large-scale SSTA from the ERSSTv5 and Z_{500}' from the NCEP1 onto the two corresponding expansion coefficients of the leading SVD mode as shown in Fig. 1 (A to D).

Significance test of the regression pattern
To ascertain the significance of regression patterns, one essentially tests N local null hypothesis tests, where N is the number of grid points. However, assuming that each local null hypothesis is true can be misleading because of the many erroneous rejections that will invariably occur for real data. For this reason, climate scientists have raised concerns about the significance area of regression patterns that is often overstated because of a lack of rigorous significance testing (39, 40). Here, we further demonstrated that the statistics of the regression maps of SSTAs and Z_{500}' on tornado number anomalies over the SGP region in April (Fig. 1E) exceed the probability of being randomly significant, whereas those for May fail that test (fig. S4). For the test, we randomly shuffled the anomalous tornado number index 1000 times and calculated the regression fields between the random time series and the gridded data (SSTAs and Z_{500}'). Figure S4 shows the histogram of the correlation coefficients between the time series and both global SSTA and Z_{500}' from each grid point within 20°N to 70°N and 0°E to 360°E. In April, the percentages of the number of grid points that exceed both the random mean (black line) and the 95% level of the two-tailed test (green lines) are more than 5.6% of the total grid points for Z_{500}' and 11.9% for SSTA.

None of the grid points in May exceeds even 3% of the statistically significant grid points.

SUPPLEMENTARY MATERIALS

REFERENCES AND NOTES

1. C. M. Fuhrmann, C. E. Konrad II, M. M. Kovach, J. T. McLeod, W. G. Schmitz, P. G. Dixon, Ranking of tornado outbreaks across the United States and their climatological characteristics. *Weather Forecast.* **29**, 684–701 (2014).
2. H. B. Bluestein, in *Severe Convective Storms and Tornadoes: Observations and Dynamics* (Springer Berlin Heidelberg, 2013), pp. 307–416.
3. H. E. Brooks, J. W. Lee, J. P. Craven, The spatial distribution of severe thunderstorm and tornado environments from global reanalysis data. *Atmos. Res.* **67-68**, 73–94 (2003).
4. B. T. Smith, R. L. Thompson, J. S. Grams, C. Broyles, H. E. Brooks, Convective modes for significant severe thunderstorms in the contiguous United States. Part I: Storm classification and climatology. *Weather Forecast.* **27**, 1114–1135 (2012).
5. K. H. Sparrow, A. E. Mercer, Predictability of US tornado outbreak seasons using ENSO and northern hemisphere geopotential height variability. *Geosci. Front.* **7**, 21–31 (2016).
6. A. E. Mercer, C. M. Shafer, C. A. Doswell III, L. M. Leslie, M. B. Richman, Synoptic composites of tornadic and nontornadic outbreaks. *Mon. Weather Rev.* **140**, 2590–2608 (2012).
7. L. Curtis, Midlevel dry intrusions as a factor in tornado outbreaks associated with landfalling tropical cyclones from the Atlantic and Gulf of Mexico. *Weather Forecast.* **19**, 411–427 (2004).
8. S. J. Weaver, S. Baxter, A. Kumar, Climatic role of North American low-level jets on U.S. regional tornado activity. *J. Clim.* **25**, 6666–6683 (2012).
9. E. Muñoz, D. Enfield, The boreal spring variability of the intra-Americas low-level jet and its relation with precipitation and tornadoes in the eastern United States. *Clim. Dyn.* **36**, 247–259 (2011).
10. B. S. Barrett, B. N. Henley, Intraseasonal variability of hail in the contiguous United States: Relationship to the Madden-Julian oscillation. *Mon. Weather Rev.* **143**, 1086–1103 (2015).
11. B. S. Barrett, V. A. Gensini, Variability of central United States April-May tornado day likelihood by phase of the Madden-Julian oscillation. *Geophys. Res. Lett.* **40**, 2790–2795 (2013).
12. D. B. Thompson, P. E. Roundy, The relationship between the Madden-Julian oscillation and US violent tornado outbreaks in the spring. *Mon. Weather Rev.* **141**, 2087–2095 (2013).
13. S.-K. Lee, R. Atlas, D. Enfield, C. Z. Wang, H. Liu, Is there an optimal ENSO pattern that enhances large-scale atmospheric processes conducive to tornado outbreaks in the United States? *J. Clim.* **26**, 1626–1642 (2013).
14. S.-K. Lee, A. T. Wittenberg, D. B. Enfield, S. J. Weaver, C. Wang, R. Atlas, US regional tornado outbreaks and their links to spring ENSO phases and North Atlantic SST variability. *Environ. Res. Lett.* **11**, 044008 (2016).
15. J. T. Allen, M. K. Tippett, A. H. Sobel, Influence of the El Niño/Southern Oscillation on tornado and hail frequency in the United States. *Nat. Geosci.* **8**, 278–283 (2015).
16. C. Lepore, M. K. Tippett, J. T. Allen, ENSO-based probabilistic forecasts of March-May US tornado and hail activity. *Geophys. Res. Lett.* **44**, 9093–9101 (2017).
17. J. B. Elsner, H. M. Widen, Predicting spring tornado activity in the central Great Plains by 1 March. *Mon. Weather Rev.* **142**, 259–267 (2014).
18. E. Jung, B. P. Kirtman, Can we predict seasonal changes in high impact weather in the United States? *Environ. Res. Lett.* **11**, 074018 (2016).
19. J. M. Wallace, D. S. Gutzler, Teleconnections in the geopotential height field during the Northern Hemisphere winter. *Mon. Weather Rev.* **109**, 784–812 (1981).
20. A. G. Barnston, R. E. Livezey, Classification, seasonality and persistence of low-frequency atmospheric circulation patterns. *Mon. Weather Rev.* **115**, 1083–1126 (1987).
21. S. B. Feldstein, Fundamental mechanisms of the growth and decay of the PNA teleconnection pattern. *Q. J. R. Meteorol. Soc.* **128**, 775–796 (2002).
22. K. E. Taylor, R. J. Stouffer, G. A. Meehl, An overview of Cmip5 and the experiment design. *Bull. Am. Meteorol. Soc.* **93**, 485–498 (2012).
23. W. L. Gates, AMIP: The Atmospheric Model Intercomparison Project. *Bull. Am. Meteorol. Soc.* **73**, 1962–1970 (1992).
24. W. L. Gates, J. S. Boyle, C. Covey, C. G. Dease, C. M. Doutriaux, R. S. Drach, M. Fiorino, P. J. Gleckler, J. J. Hnilo, S. M. Marlais, T. J. Phillips, G. L. Potter, B. D. Santer, K. R. Sperber, K. E. Taylor, D. N. Williams, An overview of the results of the Atmospheric Model Intercomparison Project (AMIP I). *Bull. Am. Meteorol. Soc.* **80**, 29–56 (1999).
25. E. Kalnay, M. Kanamitsu, R. Kistler, W. Collins, D. Deaven, L. Gandin, M. Iredell, S. Saha, G. White, J. Woollen, Y. Zhu, M. Chelliah, W. Ebisuzaki, W. Higgins, J. Janowiak, K. C. Mo, C. Ropelewski, J. Wang, A. Leetmaa, R. Reynolds, R. Jenne, D. Joseph, The NCEP/NCAR 40-year reanalysis project. *Bull. Am. Meteorol. Soc.* **77**, 437–471 (1996).
26. B. Huang, P. W. Thorne, V. F. Banzon, T. Boyer, G. Chepurin, J. H. Lawrimore, M. J. Menne, T. M. Smith, R. S. Vose, H.-M. Zhang, Extended Reconstructed Sea surface Temperature, version 5 (ERSSTv5): Upgrades, validations, and intercomparisons. *J. Clim.* **30**, 8179–8205 (2017).
27. Y. Dai, S. B. Feldstein, B. Tan, S. Lee, Formation mechanisms of the Pacific–North American teleconnection with and without its canonical tropical convection pattern. *J. Clim.* **30**, 3139–3155 (2017).
28. F.-F. Jin, L.-L. Pan, M. Watanabe, Dynamics of synoptic eddy and low-frequency flow interaction. Part I: A linear closure. *J. Atmos. Sci.* **63**, 1677–1694 (2006).
29. R. Davies-Jones, A review of supercell and tornado dynamics. *Atmos. Res.* **158–159**, 274–291 (2015).
30. F. Mesinger, G. DiMego, E. Kalnay, K. Mitchell, P. C. Shafran, W. Ebisuzaki, D. Jović, J. Woollen, E. Rogers, E. H. Berbery, M. B. Ek, Y. Fan, R. Grumbine, W. Higgins, H. Li, Y. Lin, G. Manikin, D. Parrish, W. Shi, North American Regional Reanalysis. *Bull. Am. Meteorol. Soc.* **87**, 343–360 (2006).
31. M. K. Tippett, A. H. Sobel, S. J. Camargo, Association of US tornado occurrence with monthly environmental parameters. *Geophys. Res. Lett.* **39**, L02801 (2012).
32. M. K. Tippett, A. H. Sobel, S. J. Camargo, J. T. Allen, An empirical relation between U.S. tornado activity and monthly environmental parameters. *J. Clim.* **27**, 2983–2999 (2014).
33. A. Mercer, A. Bates, Meteorological differences characterizing tornado outbreak forecasts of varying quality. *Atmosphere* **10**, 16 (2019).
34. M. K. Tippett, Changing volatility of U.S. annual tornado reports. *Geophys. Res. Lett.* **41**, 6956–6961 (2014).
35. Z. Liu, S. Vavrus, F. He, N. Wen, Y. Zhong, Rethinking tropical ocean response to global warming: The enhanced equatorial warming. *J. Clim.* **18**, 4684–4700 (2005).
36. S. M. Verbout, H. E. Brooks, L. M. Leslie, D. M. Schultz, Evolution of the US tornado database: 1954-2003. *Weather Forecast.* **21**, 86–93 (2006).
37. P. Poli, H. Hersbach, D. P. Dee, P. Berrisford, A. J. Simmons, F. Vitart, P. Laloyaux, D. G. H. Tan, C. Peubey, J.-N. Thépaut, Y. Trémolet, E. V. Hólm, M. Bonavita, L. Isaksen, M. Fisher, ERA-20C: An atmospheric reanalysis of the twentieth century. *J. Clim.* **29**, 4083–4097 (2016).
38. J. M. Wallace, C. Smith, C. S. Bretherton, Singular value decomposition of wintertime sea surface temperature and 500-mb height anomalies. *J. Clim.* **5**, 561–576 (1992).
39. T. DelSole, X. Yang, Field significance of regression patterns. *J. Clim.* **24**, 5094–5107 (2011).
40. D. S. Wilks, On "field significance" and the false discovery rate. *J. Appl. Meteorol. Climatol.* **45**, 1181–1189 (2006).

Citation: J.-E. Chu, A. Timmermann, J.-Y. Lee, North American April tornado occurrences linked to global sea surface temperature anomalies. *Sci. Adv.* **5**, eaaw9950 (2019).